International Conference on Space Optics—ICSO 2018

Chania, Greece

9–12 October 2018

Edited by Zoran Sodnik, Nikos Karafolas, and Bruno Cugny

Characterization by OCT of a new kind of micro-interferometric components for the NanoCarb miniature imaging spectrometer

Hélène Ehrhardt

Silvère Gousset

Jumana Boussey

Marie Panabière

et al.

Characterization by OCT of a new kind of micro-interferometric components for the NanoCarb miniature imaging spectrometer

Hélène Ehrhardt*[a], Silvère Gousset [a], Jumana Bousssey[b], Marie Panabière[b], Etienne le Coarer [a], Laurence Croizé[c], Yann Ferrec[c], and Laure Brooker[d] for the SCARBO consortium
[a]Institute of Planetology and Astrophysics of Grenoble (IPAG), Grenoble-Alpes University, Grenoble, France; [b]Microeletronics Technology Laboratory (LTM), LTM/UGA-CNRS CEA-Leti, Grenoble, France; [c]ONERA/DOTA, BP 80100, chemin de la Hunière, FR-91123 Palaiseau, France; [d]Airbus Defence and Space, Toulouse, France

ABSTRACT

In this paper, we describe the NanoCarb concept as well as its key elements. Then we will explain the design of the prototype followed by the development of characterization techniques. Finally, we will present how this tool can be used as part of end-to-end model. The key element of the NanoCarb concept is a matrix of silicon Fabry-Perot micro-interferometers, which allows us to perform both imaging and interferometry with a field of view of 18° and several interferometric samples in a snapshot. This technique permits us to optimize the SNR for a much reduced volume. The very complex and unusual design of this component brings huge optical and technological challenges, and requires the development of characterization techniques at the nanometer scale. Upon achievement of this purpose, the next step will be the integration of this matrix in a NanoCarb prototype to demonstrate its effective performances. We present a test bench using the interferential metrology technique of Optical Coherence Tomography (OCT). In a first time, we managed to obtain optical path maps of different silicon wafers with nanometer accuracy. Then, we employed the technique to characterize the first micro-interferometers. In parallel, we realized the first prototype integration of NanoCarb with an InGaAs focal plane array and started its characterization

Keywords: Green-house gasses monitoring, Miniaturized imaging spectrometer, Novel optical systems design, Metrology for interferometers, Optical Coherence Tomography (OCT) characterization , Detectors.

1. INTRODUCTION

The objective of the Space CARBon Observatory (SCARBO) European project is to conduct a global monitoring of the Earth's atmosphere for the measurement of human CO2 emissions at an affordable cost. This project is a feasibility study which includes a hybrid constellation composed of innovative instrument concept. All the instruments will be miniature concept embarked onboard dozens of nanosatellites of the constellation. With that kind of satellite deployment, we increase the Earth spatial coverage and the frequency of revisit.

The instruments embarked in the constellation of nanosatellites are very compact payloads. So we develop a miniaturized and low cost payload for GHG measurement: the NanoCarb concept (Gousset *et al* [1]). This instrument is collaboration with the National Office for Aerospace Studies and Research (ONERA) with a common patent. Nanocarb offers large swath (150-200 km), as well as high spatial resolution (2-3 km) and high spectral resolution (3000 <R <5000) for a weight of few kilograms, which makes it fulfil for miniature space applications. The NanoCarb concept may represent a breakthrough in terms of size, mass and power. It is based on two main features:

- It uses a very compact static imaging interferometer. The principle is presented in this conference by Ferrec *et al* [2].

- It measures only a partial interferogram also presented in this conference by Gousset *et al* [3] .

The measurement of only a partial interferogram allows us to improve both spatial coverage and spectral resolution. Regarding the interferometer, we use a low finesse integrated Fabry-Perot formed by simple silicon slides for which Fresnel reflections play role of semi-transparent faces that approach a natural two waves interferometer and allow us to work in Fourier space.

The interferometer is one feature that makes NanoCarb an unusual instrument named ImSPOC (Imaging Spectrometer On Chip). Indeed, these two ideas are combined in the instrument through a lenslet array: the interferometric plate has step case shape, so that in front of each microlens there is a parallel plate with a fixed thickness, and consequently a fixed optical path difference (OPD). Thus, we obtain a set of small images of the same scene on the focal plane array (FPA) modulated by Fabry-Perot rings, each associated with a different interferometer thickness. After image registration, we can retrieve the partial interferogram for each ground point (see Figure 1). To validate the performances of such an instrument, a first prototype will be developed within the framework of SCARBO project (see Section 3.). This prototype will be designed for an airborne campaign which will occur at the end of the project.
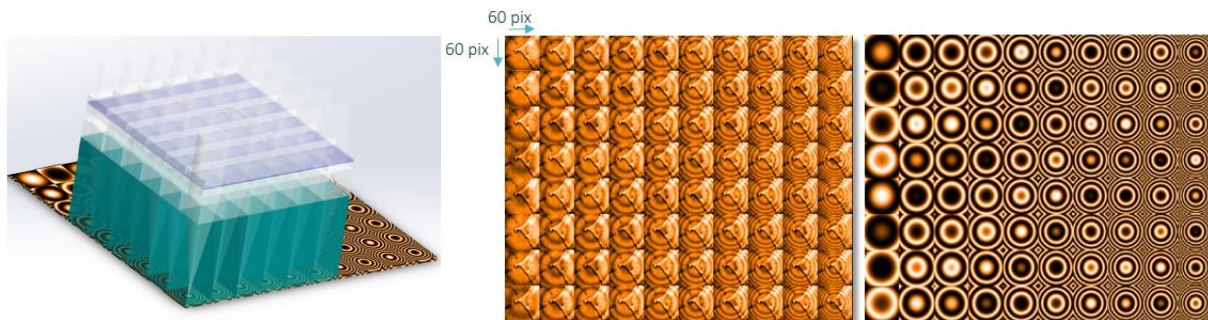

Figure 1. On the left: Interferometer (micro-lenses + FP Silicon slides), On the middle : Multiple small images of field of view modulated by Fabry-Perot rings on the detector. On the right : monochromatic Fabry-Perot rings corresponding to selected OPD around maximum sensity detection of CO2 concentration
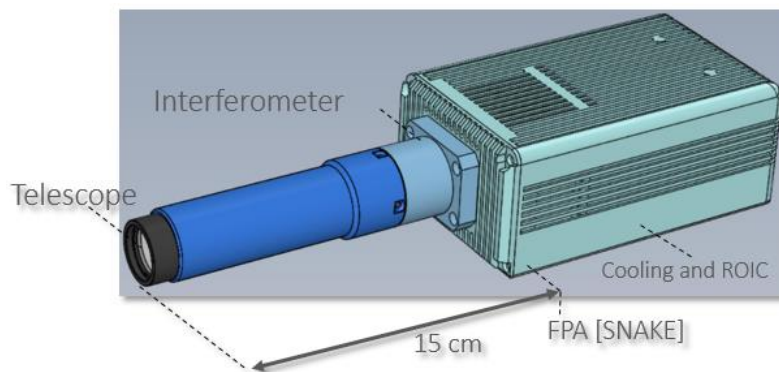

Figure 2. Schematics of NanoCarb infrared prototype with prefocal optics masking observed field of view to avoid thumbnail overlapping and adapting scale of field of view to ImSPOC sampling
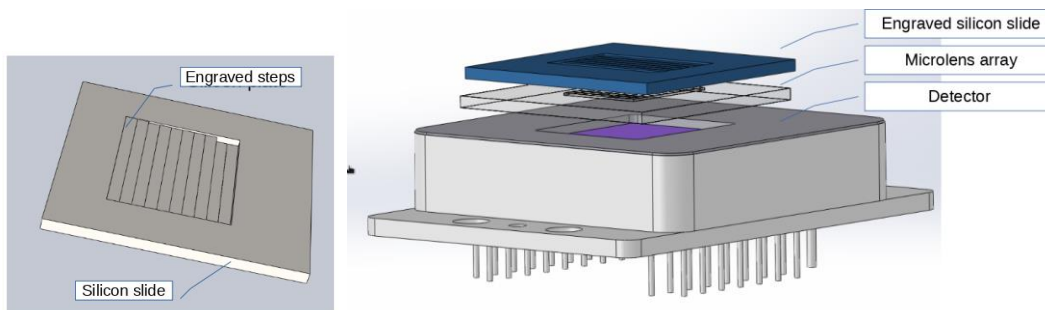
Figure 3. NanoCarb Engraved silicon slide is placed in front of microlens array. Each microlens sees an unique spaced Fabry-Perot which make an annealed Fabry-Perot figure over series thumbnail of field of view (see Figure 1) .

The slides specific engraving bring significant optical specifications: wavefront must not be disrupted by Fabry-Perot interferometer defects to insure an optical quality of images and a good interferences sampling.

These specifications require to develop characterization techniques for this particular component. All the results from the characterizations tests are inserted into an end-to-end Model to predict the instrument performances and to develop a calibration strategy.

The NanoCarb demonstration needs a performance assessment. That is why on the one hand, we develop an inverse model for measurement simulation (this method is explained in another presentation: S. Gousset et al. [3] ., "NanoCarb part 2: Performance assessment for daily CO2 monitoring from nano-satellites"), in addition to the end-to-end model with experimental inputs. On other hand, we conduct laboratory and in situ demonstration of NanoCarb.

This paper focuses on the development of a realistic instrumental model of NanoCarb, based on laboratory calibration and measurement of the device. We describe the NanoCarb concept as well as its key element. Then, we explain the instrument experimental characterization. And finally, we present simulation models and our results.

2. NANOCARB DESIGN

2.1 Instrument principle/functioning

NanoCarb is an ultra-compact static Fourier transform imaging spectrometer developed for high resolution (R ~ 5000) and greenhouse gas spectroscopy. The instrument acquires an image of 60x60 pixels and the spectral information of each point of the image. An optic focuses the rays on the interferometer of the instrument composed of an engraved silicon slide and micro-lenses. The image is then decomposed into multiple small images of the same scene observed on the detector.

Each image is modulated by a Fabry-Perot interferometer which introduces a known Optical Path Difference (OPD) (Figure 1). And the most efficient way to acquire information on CO2 is to acquire the interferogram only around this OPD. Then, spectral information of each point of the image is collected to find the CO2 concentration. We use a particular method which is the partial interferometric sampling strategy, targeting information in Fourier space (this method is explained elsewhere by Gousset *et al* [3]).

The NanoCarb prototype shown in Figure 2 is developed in laboratory for a succession of characterization tests. A lens composed of prefocal optics is placed in front of the interferometer, which is itself placed in front of the detector, see Figure 4. The infrared SNAKE detector is cooled and temperature controlled. Each element of the instrument is individually characterized.
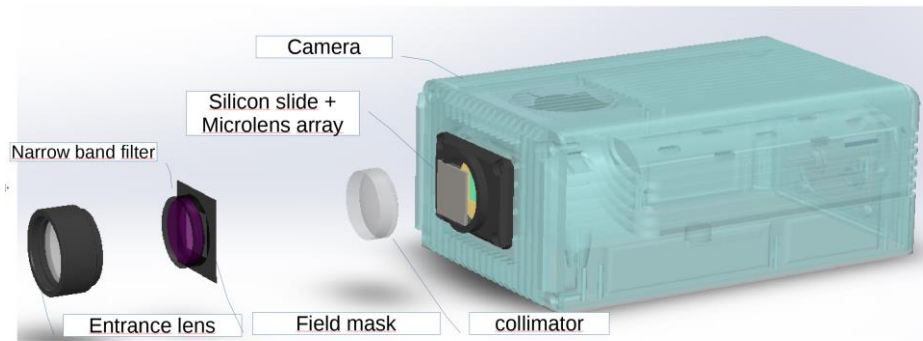
Figure 4 Sketch of optics for the Nanocarb instrument.

2.2 Interferometer description

Each Fabry-Perot interferometer is engraved in a silicon interferometric slide for CO2 detection. The interferometer is the key element of NanoCarb technology. This innovative component allows us to perform both imaging and interferometry with a field of view of 18° and several interferometric samples in a snapshot. This technique permits us to optimize the SNR for a much reduced volume. This type of engraved structure permits to sample several interference states around one OPD. These interference states give us the essential information for the CO2 measure or important geophysics/atmospheric parameter. That's why the interferometric slide development is the key success factor of the instrument.

The very complex and unusual design of the interferometric component brings huge optical and technological challenges and requires the development of a digital performance model. In this model are inserted characterization step results and experimental calibration. We developed very precise characterization techniques to meet nanometer scale precision required on engraving slides.

2.3 Interferometric slides tolerances

These slides are manufactured with microelectronic techniques for silicon, but the unusual design of the slides requires the development of particular engrave method. We need interferometric slides with an optical quality, before and after engrave to insure (RMS tolerance values). That's why we have to characterize the evolution of the intrinsic quality of silicon wafers with the engraving of the structure. A first tolerance is given on the absolute thickness of interferometer for which we want to optimize the sensitivity of CO2 detection. The Figure 5 illustrates the knowledge of the mechanical thickness should remain in a 20 µm around 825µm.
In other hands, the irregularities of silicon surfaces have two main impacts:
- Degradation of interferometric contrast of Fabry-Perot that we want to limit to 5% which corresponds roughly to 15nm (p-v) and 10nm RMS
- Deformation of transmitted wavefront that causes a degradation of PSF of associated microlens are similar.
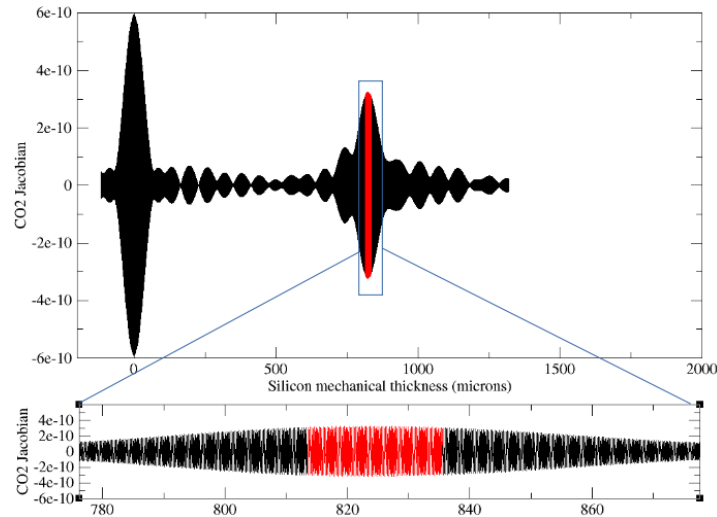
Figure 5. Jacobian of the CO2 molecule is the sensitivity to a variation of CO2 concentration of 1ppm . This jacobian is plotted along the width of interferometer. In red, the ideal silicon depth is comprised between 817µm and 835µm which seems to be not difficult to achieve.

3. EXPERIMENTAL CHARACTERIZATION

3.1 Optical Coherence Tomography (OCT) characterization

We implemented a metrology mean for interferometric slides optical characterization. This characterization bench is Michelson interferometer used for OCT (Optical Characterization Tomography) interferential metrology technique. With this instrument we can characterize slides dimensions and silicon quality. The same equipment will serve also to calibrate instrument. Contrary to Classical OCT systems popularized by Huang *et al.* [4], the optical system in set in transmission arm just before detector. This configuration permits lot of characterizations from detector, optical componants such filter or interferometers up to whole instrument itself.

The characterization bench is in infrared configuration using the instrument detector itself, composed of several light sources such laser, DFB, SLED or tungsten lamp depending of type of tests, the Michelson interferometer separating the beam and the sensor collecting the recombined beam. The mobile arm of the Michelson interferometer is composed of a 100mm delay line that we can remote control. The delay line moving steps are precise on the nanometer scale; this allows us to make data acquisition with high spatial and spectral resolution.
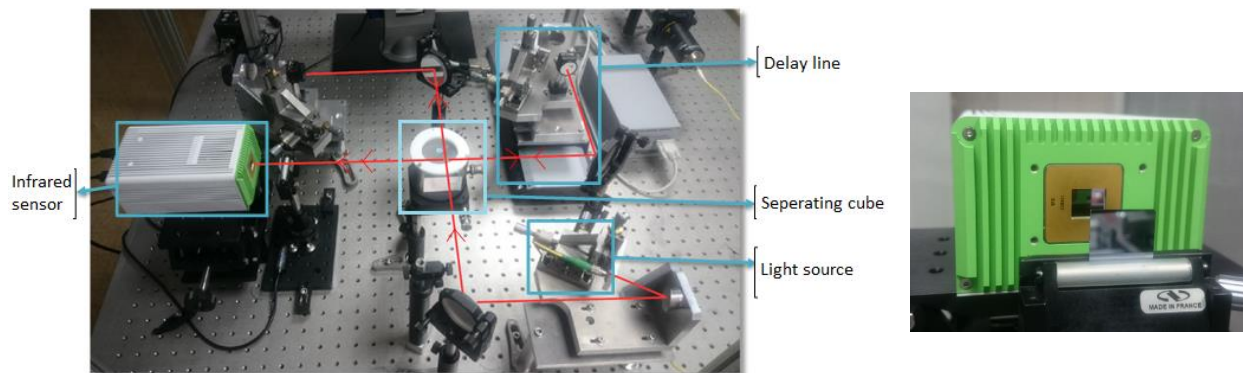

Figure 6. On the left: OCT characterization bench. On the right: Silicon slides placed in front of the infrared detector.

Indeed, our objective is to obtain very precise thickness map of the optical component. For that, we insert the silicon slides in the characterization bench, placed right before the sensor. The slides create two groups of interference fringes symmetrical about the optical contact fringes. The distance separating the two groups give us the slide thickness information. So we move the delay line around the two groups to introduce an optical path difference (OPD) and acquire the interferometric signal.
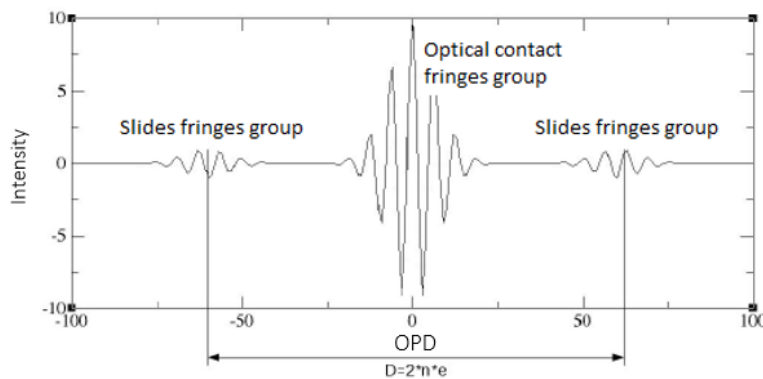

Figure 7 Interferogram obtained after moving the delay line to the position corresponding to the OPD introduced by silicon slides.

3.2 Data acquisition and processing

Thanks to a scan of the delay line, we acquire two interferograms on both slides of the optical contact, located of the two groups of fringes as shown on Figure 7. For each one, an image of the pupil is acquired at each step of the scan, with a typical $\lambda/4$ sampling of the fringes. Consequently, we obtain two cubes of data to process. The Figure 8 shows a raw acquired image for one of the two cubes, and the extracted interferogram over a region of the pupil.
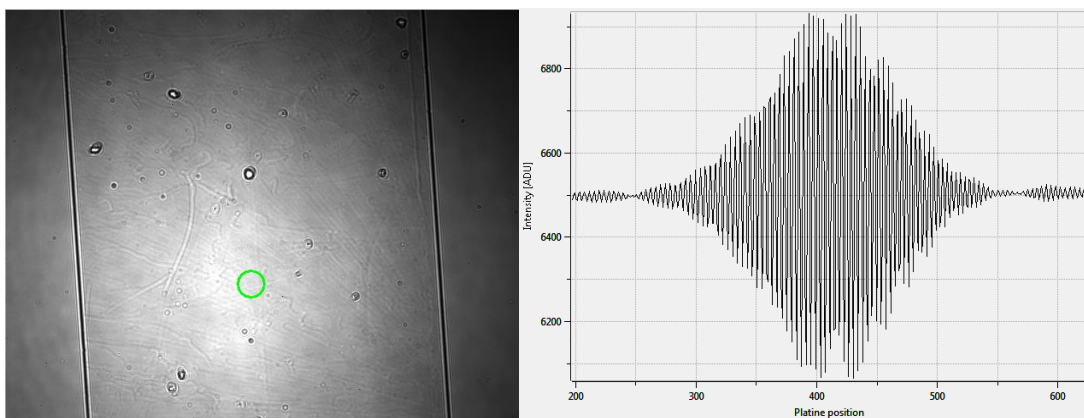

Figure 8 Left: raw image of the pupil intensity, for a given position of the delay line. The silicon plate we scan is 500 nm depth engraved in a rectangular area. The image shows the two diffracted parallel edges of this area. Right: extracted interferogram from the green-circled area, as a function of the position of the delay line device.

The Figure 8 lets appear several illumination in-homogeneities over the pupil, cause by source speckles or dusts over the optics. We achieve a pre-processing of the data cube with a flat-normalization, as a result presented on Figure 9. Several fringes are visible, due to a tilt between reference line and delay line of the Michelson. This allows also to notice as expected a phase-shift across the frontier between engraved area and native area. We will explain now how we quantify this shift.
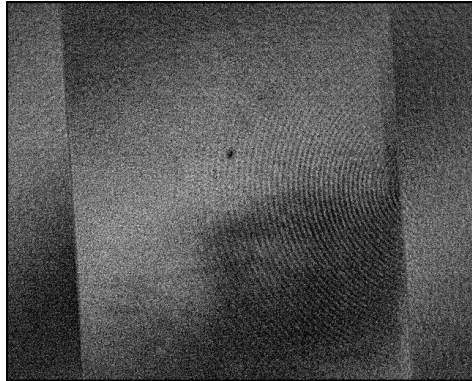
Figure 9 Normalized single image of one of the interferometric data cubes. The intensity variations over the image are due to interferences, introduced both by a tilt in the Michelson and by structure variations in the scanned silicon plate.

We extract the interferogram for each pixel of the pupil and then we process it. We combine two types of processing over the acquired data cubes:

- Cross-spectrum method for fine relative phase variations on the plate.

- Low resolution envelope detection for absolute thickness measurement, using the encoder position of the delay line.

The cross-spectrum method consists in a measurement of the phase above the intensity spike of the inter-correlation Fourier Transform, between a given pixel and a reference zone as presented on the Figure 10. We subtract the two obtained phase maps (for the two groups of fringes), to derive a relative phase map variations over the pupil, debiased of the bench aberrations.
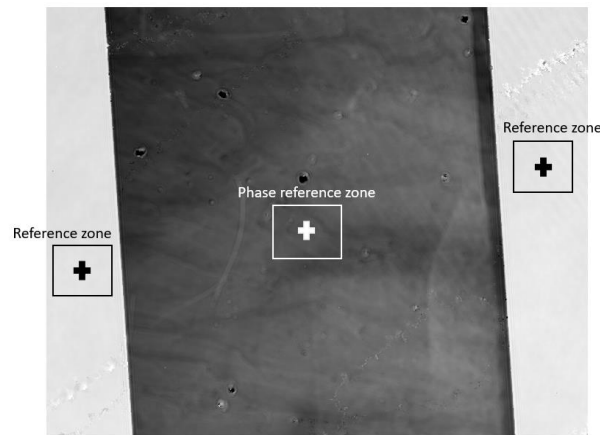

Figure 10 Relative phase variation map obtained with the cross-spectrum method. The phase variations are given with respect to the reference position.

Nevertheless, we cannot derive an absolute thickness measurement of the plate with the cross-spectrum method. Furthermore, a plate structuration can induce some misestimate of the phase variation, because a continuity assumption is required for an un-wrap of the phase. For example, on the Figure 10, the 500nm-engraving is too important to un-wrap the phase with a continuity assumption, as a result of a misestimate of the depth.

Consequently, we jointly use envelope detection over each interferogram to read maximum value of both fringe group and its delay line corresponding position. By subtracting the two maps of position we obtain the absolute OPD above each pixel. This method is less accurate because we use the mechanical position returned by the delay line, as well as we use a centroid estimate over the envelope to derive the relevant thickness.

This absolute thickness is averaged over the different areas of the structured plate, and combined to the fine phase variation map as illustrated on Figure 10. The obtained map shows both nanometer-scale variations and large µm-structures.

The combination of the phase map and of the absolute OPD requires evaluating the mean wavelength of the source, while we need to assume the averaged optical index of the silicon to derive the mechanical thickness maps. The source wavelength is jointly evaluated on the Michelson by a Fourier Transform of the interferograms. Both this wavelength and temperature room are used to assume an effective optical index of the plate.

3.3 Obtained thickness maps

We present in this sub-section the obtained OCT maps of thickness. The sources of errors are assessed in characterization experiments. We measure two kinds of processed silicon samples:

- Thinned silicon by grinding technic, investigating our capability to target a given OPD over the interferogram with NanoCarb.

- Engraved silicon plate by lithography, assessing the accuracy to sampling the interferogram with controlled step.

OCT measurement results are presented on Figure 11. The absolute thickness measurement is 850 µm, for an 825 µm target. Joint mechanical measurements give 825 µm. A preliminary error budget analysis allows us to discard some experimental OCT biases. Some issue concerning constrains over the silicon during processing are investigated. Furthermore, the thinned plate presents a prismatic profile around 500 nm across the green line plotted on Figure 11. RMS values of the squared areas are reported in the Table 1. The squared are 64x64 pixels, comparable to NanoCarb thumbnail typical size. On the left full map, the RMS value is dominated by prismatic shape of the plate. A typical value of 10 nm is obtained remaining in tolerance budget in (p-v). We subtract the prismatic shape in the right-map, allowing to derive a RMS value around 1 nm => Thinned processing induces large variation over the plate, but has a good roughness. The observed structures over the right map seem to be induced by volumetric inhomogeneities of refractive index. We can note that it is more important for NanoCarb to measure a real optical thickness rather mechanical one.
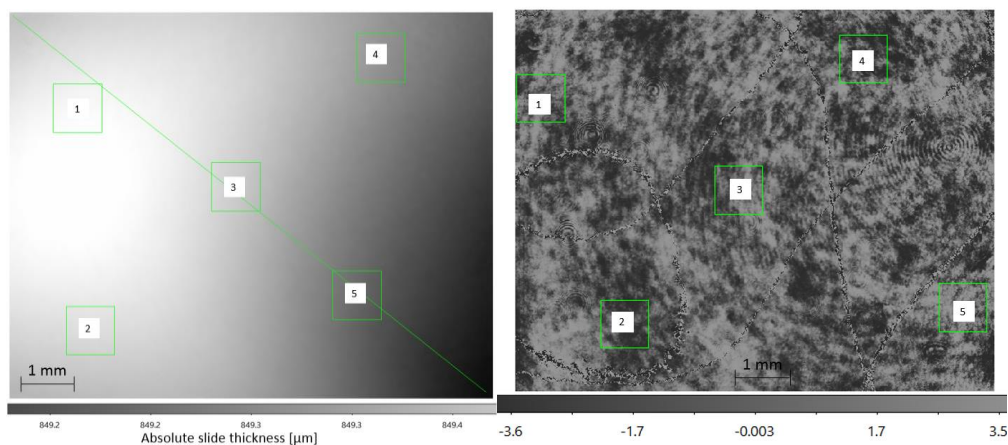

Figure 11 Thinned silicon sample. Left: combined absolute thickness map. Right: fine OPD variations.

Table 1 RMS value of OPD variations, in unit of mechanical nanometer

Region	Figure 11-left (p-v)	Figure 11-right (RMS)
1	9.2	1.8
2	14.2	2.6
3	18.6	1.7
4	16.9	2.3
5	21.9	2.1

Measured map in a first sample visible on Figure 12, showing an engraving around 380 nm for a target of 500 nm. A lithography issue is responsible for this bias, as well as a RMS value in the engraved area (square 2 3 and 4) around 10 nm compare to a 1 nm RMS value for the native area (1 and 5).
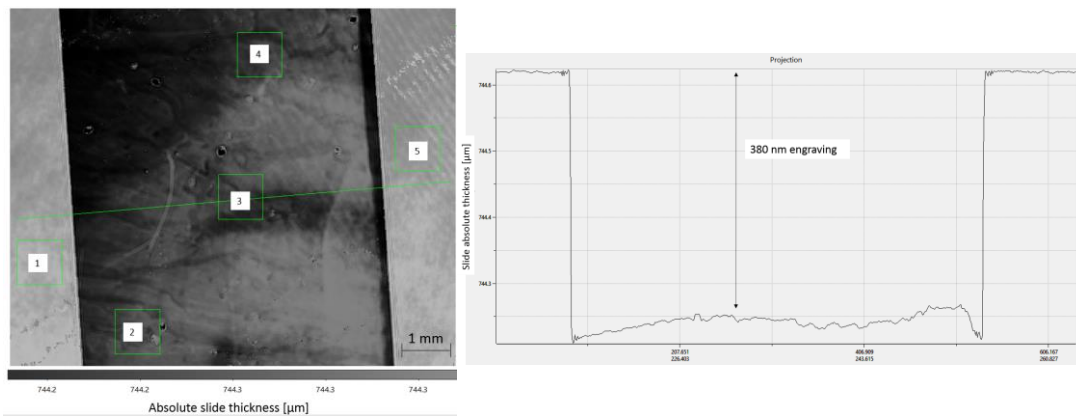

Figure 12 First engraved sample of silicon. Left: combined absolute thickness map. Right: profile of the absolute thickness map across the green line.

The second tested sample for the engraving technic is more promising as shown on Figure 13, with a closer 500 nm engraving area and a RMS value around 1 nanometer, comparable inside and outside the engraved area. Thus, the engraving process seems to not degrade the quality of the interferometer, with an accurate profile of depth.
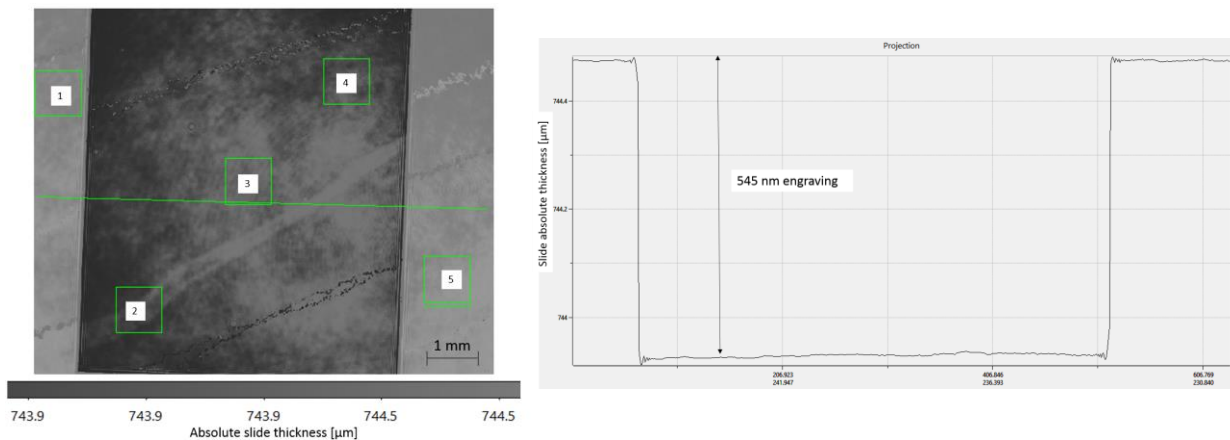

Figure 13 Second engraved sample of silicon. Left: combined absolute thickness map. Right: profile of the absolute thickness map across the green line.

4. SIMULATIONS

Objectives of this tool is to feed an end to end model in order to provide complete instrument simulator such it has been done for PICTURE-C mission by Douglas et al. [5] . We are writing a special python WFE module compatible with POPPY toolbox [6] with the goal to progressively replace theoretic elements by measured real one. Figure 14 illustrates simulation which can be done from slides thickness measurements. Arbitrary zone 3 and 5 from Figure 13 representing two extreme cases often dominated by (p-v).
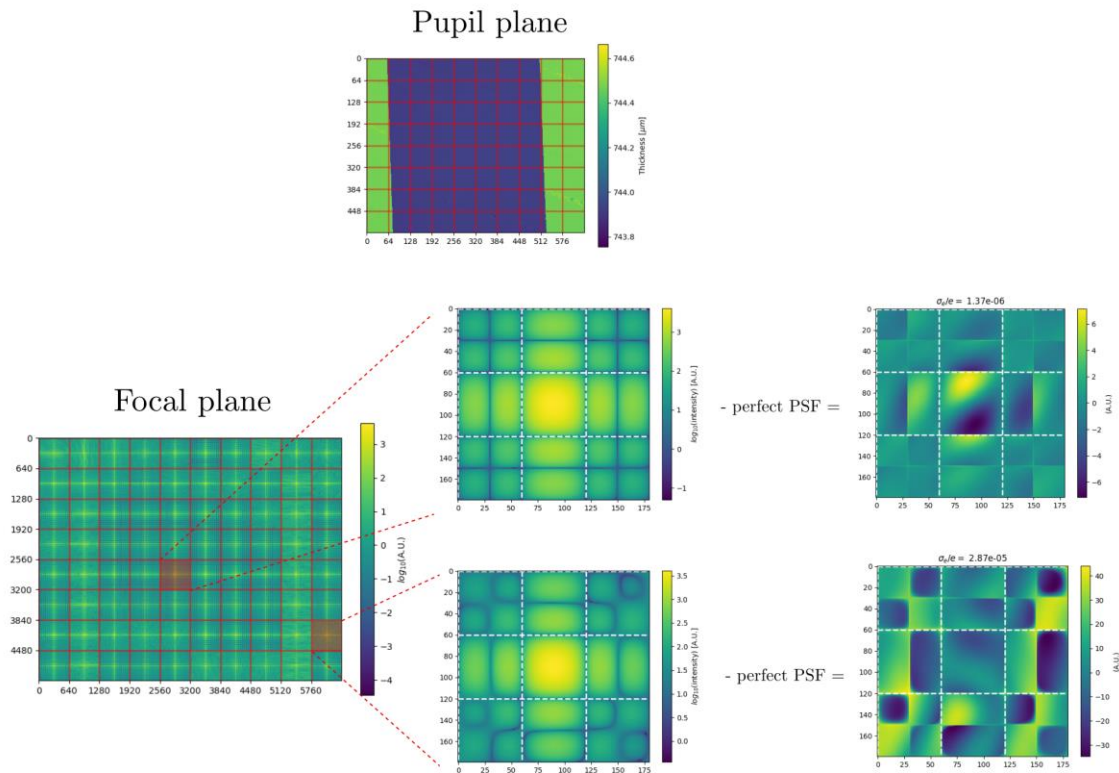
Figure 14. Example of calculated square microlens array PSF at detector level introduced by silicon slide inhomogeneities. Up: At pupil plane of second engraved sample of silicon slide used for Figure 13 (upside and downside exchanged). Down left : oversampled image with two test zones (Zone 3 and 5) for which is plotted logarithm of intensity of PSF and a linear scale of the difference with the perfect PSF. In the best case, this difference is roughly 1/1000 dominated by tilt aberration. The worst case in lateral zone for which the difference can reach 1/100 of the central flux.

5. CONCLUSION

We presented here the current NanoCarb instrument design. The OCT bench development answers to the necessity to have tools to control optical quality along instrument assembling, integrations and tests. The OCT bench is a very promising tool that can be used for lot of characterizations from critical optical pieces to instrument itself including its detector. This bench is built to produce necessary information enforcing the end-to-end model. A preliminary example of simulation of resulting PSF using first results permits us to show that it is well adapted to critical characterizations of interferometer's thickness, surfaces and induced image quality. With these very first tests we can verify that lithography or grinding technics can provide a right surface quality.

REFERENCES

[1] Gousset, S., Le Coarer, E., Guérineau, N., Croizé, L., Laveille, T., & Ferrec, Y. (2017, September). NANOCARB-21: a miniature Fourier-transform spectro-imaging concept for a daily monitoring of greenhouse gas concentration on the Earth surface. In International Conference on Space Optics—ICSO 2016 (Vol. 10562, p. 105624U). International Society for Optics and Photonics.

[2] Ferrec, Y, Bonnery, G, Brooker, L, Croizé, L, Gousset, S, Le Coarer, E, and the SCARBO consortium, "NanoCarb part 1: Compact snapshot imaging interferometer for CO2 monitoring from space", Proc. of International Conference on Space Optics ICSO2018 (2018)

[3] Gousset, S., Croizé, L., Le Coarer, E., Ferrec, Y., Brooker, L., and Scarbo consortium, "NanoCarb part 2: Performance assessment for total column CO2 monitoring from a nano-satellite," Proc. of International Conference on Space Optics ICSO2018 (2018)

[4] Huang, D., Swanson, E. A., Lin, C. P., Schuman, J. S., Stinson, W. G., Chang, W., ... & Puliafito, C. A. (1991). Optical coherence tomography. Science, 254(5035), 1178-1181.

[5] Douglas, E. S., Hewawasam, K., Mendillo, C. B., Cahoy, K. L., Cook, T. A., Finn, S. C., ... & Mawet, D. (2015, September). End-to-end simulation of high-contrast imaging systems: methods and results for the PICTURE mission family. In Techniques and Instrumentation for Detection of Exoplanets VII (Vol. 9605, p. 96051A). International Society for Optics and Photonics.

[6] Perrin, M. D., Soummer, R., Elliott, E. M., Lallo, M. D., and Sivaramakrishnan, A., "Simulating point spread functions for the James Webb Space Telescope with WebbPSF," in [Proc. SPIE], 8442, 84423D– 84423D–11 (2012).

ACKNOWLEDGEMENTS